ACS APPLIED NANO MATERIALS

www.acsanm.org Article

Graphene-Like Matrix Composites with Fe_2O_3 and Co_3O_4 as Cathode Materials for Lithium−Sulfur Batteries

Pengyu Wang,[#] Rong Zeng,[#] Lei You, Hu Tang, Jiasong Zhong,* Shiquan Wang, Tao Yang,* and Jianwen Liu*

Cite This: *ACS Appl. Nano Mater.* 2020, 3, 1382−1390 Read Online

ACCESS | Metrics & More | Article Recommendations | Supporting Information

ABSTRACT: As promising next generation battery systems, the future practical application of lithium−sulfur batteries has been restricted by their low conductivity and the shuttle effect of polysulfides. To solve these issues, herein we design a three-dimensional graphene-like matrix composited with nanoscale iron oxide as a host for sulfur, which can be easily synthesized from citric acid under the reaction of ferric chloride via a simple one-step route. The as-prepared graphene-like matrix with a large specific surface area and an ordered space structure can host more sulfur, provide more space for sulfur expansion, and improve electrical conductivity. In addition, the polar nitrogen and iron oxide nanoparticles uniformly distributed on the surface of the carbon sheet strongly adsorb polysulfides to minimize the shuttle effect. On the basis of the above design, the electrode delivers an initial specific capacity of 1196 mA h g^{-1} at 0.1C and a discharge capacity of 829 mA h g^{-1} at 0.5C after 300 cycles. This work will provide a promising direction for high performance lithium−sulfur batteries, especially in practical industrialization applications.

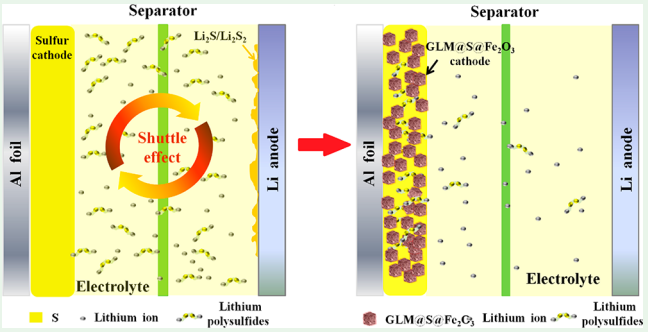

KEYWORDS: *lithium−sulfur batteries, graphene-like structure, nanoscale metal oxide*

1. INTRODUCTION

Currently, commercial lithium ion batteries with a low energy density and battery capacity are unable to meet the strict requirements of electric vehicles and for large scale energy storage.[1] Lithium−sulfur (Li−S) batteries, with a high theoretical energy density of 2500 W h kg^{-1} and capacity of 1675 mA h g^{-1}, have been recognized as the most promising candidate for next-generation battery systems.[2,3] However, during battery charge and discharge, elemental sulfur and discharge products (Li_2S/Li_2S_2) show nonconductive characteristics at room temperature. Worse still, the intermediate lithium polysulfide products (Li_2S_n, $n \geq 4$) are easily soluble in electrolytes, which is the so-called "shuttle effect" that leads to the severe loss of irreversible capacity.[4−6]

On the basis of recent literature, physical confinement methods are first applied to Li−S batteries, including the use of carbon-coated methods or porous materials as a host for sulfur.[7−9] On the basis of physical confinement, the problems of volume expansion and low conductivity can be solved efficiently, but most of the lithium polysulfides can still dissolve into electrolytes. Therefore, chemical adsorption methods are used to further improve the electrochemical performance of Li−S batteries by compounding them with N-doped or S-doped carbon,[10−12] conducting polymers,[13,14] metallic oxides,[15−19] metallic nitrides,[20,21] metallic sulfides,[22−24] and metal−organic frameworks[25,26] in the electrode to adsorb the polysulfides. Among the host materials, carbon-based materials with a large specific area have been developed as the most promising sulfur host to solve these problems by offering a favorable electronic conductivity and an effective polysulfide confinement. Carbon aerogel,[27,28] carbon nanotubes,[29−32] porous graphene,[33−37] and biomass-derived carbon[38,39] were especially used as host materials for Li−S batteries. For example, Kai et al. designed an ideal graphene structure for a Li−S battery by using advanced 3D printing technology, which yielded an excellent cycling stability.[40] Additionally, Yoon et al. prepared the sulfur, graphene oxide (GO), and carbon nanotube (CNT) composites by means of simple freeze-drying, which showed a high sulfur loading and a high initial capacity.[41]

Table 1 summarizes the electrochemical properties of carbon materials composited with chemical mediators (mainly metal oxides) used in recent years. Many metal oxides (including TiO_2, MnO_2, MoO_2, MgO, Co_3O_4, NiO, etc.) have been applied to the cathode of lithium−sulfur batteries, and some have exhibited excellent electrochemical perform-

Received: November 15, 2019
Accepted: January 27, 2020
Published: January 27, 2020

https://dx.doi.org/10.1021/acsanm.9b02250
ACS Appl. Nano Mater. 2020, 3, 1382−1390

Table 1. Performance Comparison of Carbon Materials Composited with Chemical Mediators (Mainly Metal Oxides) for Lithium−Sulfur Batteries

materials	content of sulfur (wt %)	areal sulfur mass loading (mg cm^{-2})	cycling stability (mA h g^{-1})	ref.
C@MnO_2	58.2	3.0	712 (0.5C, 300 cycles)	43
NMRC@MnO_2	72	1.8	1023 (0.2C, 200 cycles)	44
NPCFs@TiO_2	55	2.4	734 (1C, 100 cycles)	45
GN@$Ti_3C_2T_x$	75	5.1	662 (0.5C, 200 cycles)	46
MXene@TiO_2	79	1.5	680 (2C, 500 cycles)	47
CNTs@TiO_2	65	3.0	616 (0.5C, 200cycles)	48
rGO@MoO_2	70	2.4	1027 (0.5C, 500 cycles)	49
CNTs@MgO	78	14.4	426 (0.1C, 60 cycles)	50
C@Co_3O_4	42	0.8	656 (0.2C, 200 cycles)	51
C@Fe_3O_4	80	2.2	1165 (0.1C, 200 cycles)	52
C@NiO	80	2.2	682 (2C, 300 cycles)	19

ances. Among them, most studies have focused on TiO_2 and MnO_2, which could be regarded as promising candidates for use in applications. Few reports on iron oxides appear, as progress is slow in this particular area of research.[42,52]

Overall, owing to the high cost of raw materials and burdensome preparation process, the price and synthetic methods of these carbon-based materials make them unrealistic as hosts for Li−S batteries. Herein, we proposed citric acid as a simple carbon source to design a three-dimensional graphene-like matrix (GLM), composited with cheap Fe_2O_3 particles on the surface of the carbon sheets. The carbon nanosheets guarantee the level of sulfur loading and additional electrochemical active sites; in addition, the three-dimensional graphene-like structure provides conductive networks and ion channels.[53] More importantly, the polar nitrogen and Fe_2O_3 nanoparticles on the carbon nanosheets both have strong chemical interactions with polysulfides, which can effectively inhibit the shuttle effect of lithium polysulfides.[52,54] When used in the Li−S batteries, the composite presents a high sulfur loading and displays excellent reversibility and good cycle stability with an initial specific capacity of 1196 mA h g^{-1} at 0.1C and a high specific discharge capacity of 829 mA h g^{-1} at 0.5C after 300 cycles. When compared with similar state-of-the-art materials, GLM@S@Fe_2O_3 exhibits an excellent cycling performance and a high rate capacity with a high sulfur content and a general areal sulfur mass loading. As a result, the three-dimensional graphene-like structure with a GLM@S@Fe_2O_3 host shows better properties for future use in Li−S battery industrialization.

2. EXPERIMENTAL SECTION

2.1. Preparation of the GLM@Fe_2O_3 Composite. First, 7.35 g of NaCl (template), 1.25 g of citric acid ($C_6H_8O_7$, main carbon sources and pH conditioning agent), 0.25 g of polyvinylpyrrolidone ($(C_6H_9NO)_n$, minor carbon sources, nitrogen sources, and surface active agent), and 0.32 g of $FeCl_3{\cdot}6H_2O$ (iron sources) were dissolved in 40 mL of deionized water with thorough stirring for 2 h. Then, the solution was transferred into the refrigerator for 24 h freezing, followed by freeze-drying for 72 h to obtain a yellow powder. After that, the yellow powder was carbonized in an argon atmosphere with a ramp rate of 2 °C/min at 650 °C for 3 h in a tubular furnace. The product was subsequently soaked in 500 mL of deionized water, followed by vacuum filtration. After drying 60 °C overnight, the three-dimensional graphene-like matrix composited with Fe_2O_3 (GLM@Fe_2O_3) was obtained.

2.2. Synthesis of the GLM@S@Fe_2O_3 Composite. Figure 1 illustrates the synthesis process of the GLM@S@Fe_2O_3 composite in this experiment. The GLM@Fe_2O_3 sample was mixed with sublimed sulfur at a mass ratio of 1:3 and grounded for 1 h. Then, the mixture

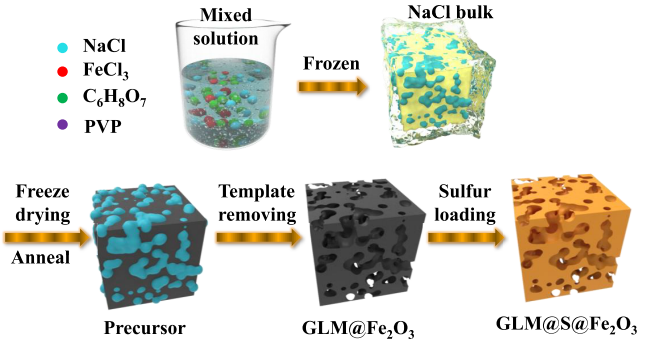

Figure 1. Schematic illustration of the synthesis process for the GLM@S@Fe_2O_3 composite in this experiment.

was heated to 155 °C in a Teflon-lined stainless steel autoclave filled with argon for 12 h to obtain the GLM@S@Fe_2O_3 composite. For comparison, the GLM@S sample without Fe_2O_3 and the GLM@S sample composited with Co_3O_4 (synthesized from $CoCl_2{\cdot}6H_2O$) hosting sulfur (GLM@S@Co_3O_4) were also obtained using the same experimental process.

2.3. Material Characterization and Electrochemical Measurements. First, the phase measurements with X-ray diffraction (XRD, D8-ADVANCE), X-ray photoelectron spectroscopy (XPS, Escalab 250X, Thermo Fisher Scientific), Raman spectroscopy (RS, Renishaw, Malvern), and thermogravimetric analysis (TGA, PERKIN ELMER, USA) were used to analyze the composition of the GLM@S@Fe_2O_3 composite. Meanwhile field-emission scanning electron microscopy (FE-SEM, Tecnai G20) and transmission electron microscope (TEM, JSM-6510LV) were adopted to investigate the morphologies of the samples.

For the battery assembly process, the GLM@S@Fe_2O_3 composite was mixed with acetylene black and polyvinylidene fluoride with a mass ratio of 8:1:1 in *N*-methyl pyrrolidone solvent to form a slurry. Then, aluminum foil was coated with the above slurry, followed by drying at 55 °C overnight to obtain the GLM@S@Fe_2O_3 electrode. For comparison, the GLM@S and GLM@S@Co_3O_4 electrodes with the same sulfur content as GLM@S@Fe_2O_3 were also manufactured, and the sulfur mass loading of all three electrodes were designed between 1.0 and 1.5 mg cm^{-2}. The quantity of the electrolyte used in a single Li−S battery was 30 μL, which was acquired by dissolving lithium bis-trifluoromethanesulfonimide ($C_2F_6LiNO_4S_2$, 1 M) and $LiNO_3$ (2.0 wt %) in a mixed solvent of 1,2-dimethoxyethane (DME) and 1,3-dioxolane (DOL) with a volume ratio of 1:1. The cell performance was tested within a voltage window of 1.7−2.8 V by a Land Battery Tester. Cyclic voltammetry (CV) and electrochemical impedance spectroscopy (EIS) were conducted by using an electrochemical workstation (CHI 660E).

https://dx.doi.org/10.1021/acsanm.9b02250
ACS Appl. Nano Mater. 2020, 3, 1382−1390

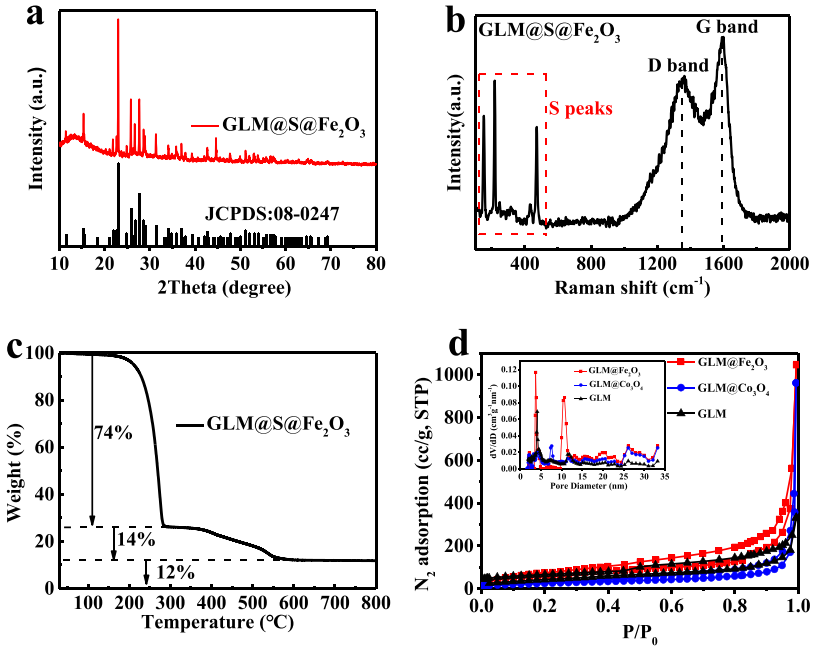

Figure 2. (a) XRD pattern, (b) Raman spectrum, and (c) TG curve in air of the GLM@S@Fe_2O_3 composite. (d) Nitrogen adsorption−desorption isotherm curves and pore size distributions of GLM@Fe_2O_3, GLM@Co_3O_4, and GLM.

3. RESULTS AND DISCUSSION

NaCl, $C_6H_8O_7$, $(C_6H_9NO)_n$, and $FeCl_3{\cdot}6H_2O$ are first dissolved together in deionized water with thorough stirring with a mixed solution pH of 2.5, and then, the citric acid and iron(III) are bonded to form $[Fe(C_6H_5O_7)]$ with a complex stability constant of $lg\beta_n$ = 11.2.[55,56] Therefore, the stable and ordered graphene-like 3D matrix structures are easily obtained after freeze-drying, template removal, and carbonation, as shown in Figure S1c and S1d. However, when replacing $FeCl_3{\cdot}6H_2O$ by $CoCl_2{\cdot}6H_2O$ in the same synthesis process, Co^{2+} only exists in the solution as an ion without bonding with citric acid.[57] During the carbonization process, the ions of Co^{2+} are reactive with molten citric acid to form Co_3O_4; meanwhile, the unordered clumps of carbon are simultaneously formed, as shown in Figure S1b. As a result, the Brunauer−Emmett−Teller (BET) surface area of GLM@Co_3O_4 is even lower than that of GLM itself, and the disorderly and unsystematic structure of GLM@S@Co_3O_4 seriously affects its electrochemistry performance.

The XRD patterns of GLM, GLM@Fe_2O_3, and GLM@Co_3O_4 composites are displayed in Figure S2. The low-intensity peaks in the patterns of GLM@Fe_2O_3 and GLM@Co_3O_4 match well with Fe_2O_3 (JCPDS No. 54-0489) and Co_3O_4 (JCPDS No. 65-3103), respectively, and the humps appearing in the pattern for GLM are attributed to the amorphous carbon from citric acid. In Figure 2a, the GLM@S@Fe_2O_3 composite displays the diffraction peaks of crystal sulfur, corresponding to standard orthorhombic sulfur (JCPDS No. 08-0247).[58] The humps at 10−20° originate from the carbon nanosheets, and the diffraction peaks of Fe_2O_3 are covered by the high-intensity peaks of sulfur. In addition, the Raman spectrum of the GLM@S@Fe_2O_3 composite is shown in Figure 2b, and the three sharp peaks below 500 cm^{-1} are due to orthorhombic sulfur. The typical peaks at ∼1345 and 1590 cm^{-1} are displayed in this spectrum, revealing the D and G bands of the graphene-like carbon nanosheets, respectively.[59−61] In order to obtain the content of sulfur in the GLM@S@Fe_2O_3, TGA was carried out under air in a temperature range of 30 to 800 °C with a ramping heating rate of 10 °C min^{-1}. As presented in Figure 2c, the mass loss of about 74% between 30 to 350 °C is attributed to the loss of sulfur, which is consistent with the result under a N_2 atmosphere shown in Figure S3, and the mass loss of about 14% from 350 to 600 °C is derived from the oxidation of carbon. Therefore, the contents of sulfur loading and carbon nanosheets are about 74% and 14%, respectively, and the remaining 12% over 600 °C is mainly due to nonvalent Fe_2O_3. The surface area and pore structure of GLM@Fe_2O_3, GLM@Co_3O_4, and GLM were obtained by nitrogen absorption−desorption isotherms. As shown in Figure 2d, GLM@Fe_2O_3 presents the largest BET surface area of 223 m^2 g^{-1} with the highest pore volume of 0.519 cm^3 g^{-1}, calculated by the nonlocal density functional theory (NLDFT) method, compared to GLM@Co_3O_4 and GLM with BET surface areas of 97 and 151 m^2 g^{-1} and pore volumes of 0.232 and 0.256 cm^3 g^{-1}, respectively. In addition, the mesoporous structures are mainly distributed in a range between 4 and 11 nm, as displayed in the inset of Figure 2d. These results indicate that the introduction of $FeCl_3$ increases the specific surface area of the material and makes the structure more stable by catalysis. The large surface area and abundant mesopores of GLM@Fe_2O_3 can guarantee the surface loading and more active sites.

The morphologies of the GLM@S@Fe_2O_3, GLM@S@Co_3O_4, and GLM@S composites can be observed in Figure 3a−3c. Compared with the disorderly sheets of GLM@S and the irregular agglomeration of GLM@S@Co_3O_4, the GLM@S@Fe_2O_3 composite displays a unique and uniform three-dimensional structure composed of ordered graphene-like carbon nanosheets with a particle size of about 20−50 nm. Moreover, the morphologies of GLM@S@Fe_2O_3, GLM@S, and GLM@S@Co_3O_4 remain almost the same as their hosts (GLM@Fe_2O_3, GLM, and GLM@Co_3O_4, respectively), as shown in Figure S1, indicating that the uniform, three-

https://dx.doi.org/10.1021/acsanm.9b02250
ACS Appl. Nano Mater. 2020, 3, 1382−1390

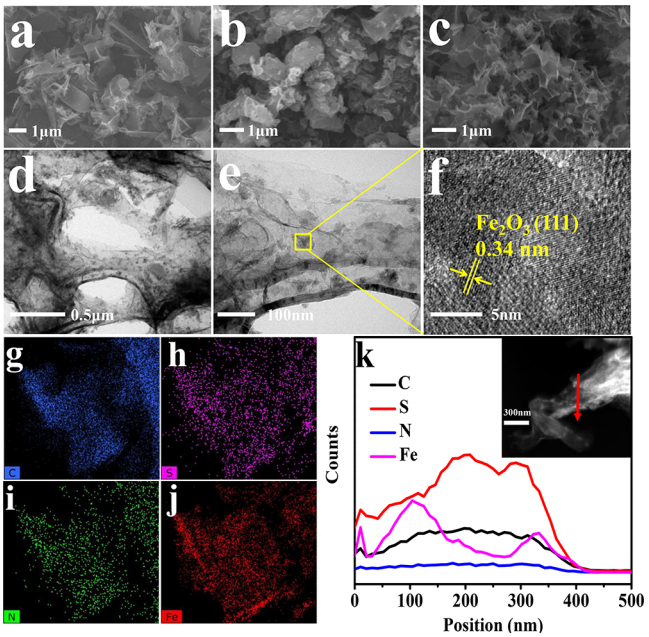

Figure 3. SEM images of (a) GLM@S, (b) GLM@S@Co_3O_4, and (c) GLM@S@Fe_2O_3 composites. (d and e) TEM and (f) HR-TEM images of the GLM@S@Fe_2O_3 composite. (g) Elemental mapping images of (g) carbon, (h) sulfur, (i) nitrogen, and (j) iron. (k) TEM image of GLM@S@Fe_2O_3 and corresponding EDS line-scanning curves of C, S, N, and Fe elements.

dimensional structure of GLM@S@Fe_2O_3 maintains its stability. As shown in the TEM images in Figure 3d and 3e, the three-dimensional structure and graphene-like nanosheets can be clearly observed, and given the ultrafine crystal lattice belonging to Fe_2O_3 in Figure 3f, Fe_2O_3 particles are shown to be uniformly distributed on the carbon nanosheets. Furthermore, the results of the elemental mapping presented in Figure 3g–3j demonstrate that sulfur and the Fe_2O_3 particles are evenly distributed in the three-dimensional matrix, and the result of the EDS line scanning further confirms that sulfur immerged into the GLM@S@Fe_2O_3 host, as shown in Figure 3k.

The XPS spectrum of the GLM@S@Fe_2O_3 composite is displayed in Figure 4a and contains the signals of C, N, O, S, and Fe. The peaks in the C 1s spectrum (Figure 4b) of GLM@S@Fe_2O_3 located at 284.56, 284.98, 285.90, and 288.52 eV correspond to the sp^2 hybridized C, C–OH species, C–N groups, and O = C–OH species, respectively.[62] The N 1s spectrum of GLM@S@Fe_2O_3 was then resolved into three peaks centered at ~400.7, ~399.8, and ~398.3 eV for nonpolar graphitic N, polar pyridinic N, and pyrrolic N, respectively. As is well-known, pyridinic N and pyrrolic N have been confirmed as key players in improving the electrochemistry performance of Li–S batteries due to their strong adsorption effect on polysulfides.[63−66] Moreover, the Fe 2p spectrum in Figure 4d displays two major peaks: Fe $2p_{1/2}$ at 724.7 eV and Fe $2p_{3/2}$ at 710.6 eV, confirming that $FeCl_3$ is completely converted to Fe_2O_3, which is consistent with the XRD pattern of GLM@Fe_2O_3.

The cyclic voltammetry (CV) curve of the GLM@S@Fe_2O_3 electrode was investigated between the voltages of 1.7 and 2.8 V at a scanning speed of 0.1 mV s^{-1}. Figure 5a shows typical CV curves of a sulfur cathode; it is obvious that the curves starts to overlap after the first cycle, suggesting the excellent stability.[67] Two obvious peaks at around 2.05 and 2.35 V correspond to the reduction of sulfur to long-chain polysulfides (Li_2S_x, $4 \le x \le 8$) and the further reduction of long-chain polysulfides to Li_2S/Li_2S_2, respectively. The two anodic peaks at around 2.4 V are related to the oxidization of Li_2S/Li_2S_2 to the long-chain polysulfides and ultimately to sulfur.[68−70] In the charge and discharge profiles of GLM@S@Fe_2O_3 in Figure 5b, the GLM@S@Fe_2O_3 electrode presents more stable overlapping than the GLM@S@Co_3O_4 in Figure 5c and GLM@S in Figure 5d, indicating the better electrochemical reversibility and stability of the GLM@S@Fe_2O_3 electrode. In addition, compared with the potential difference between the charge and discharge plateaus of the GLM@S and GLM@S@Co_3O_4

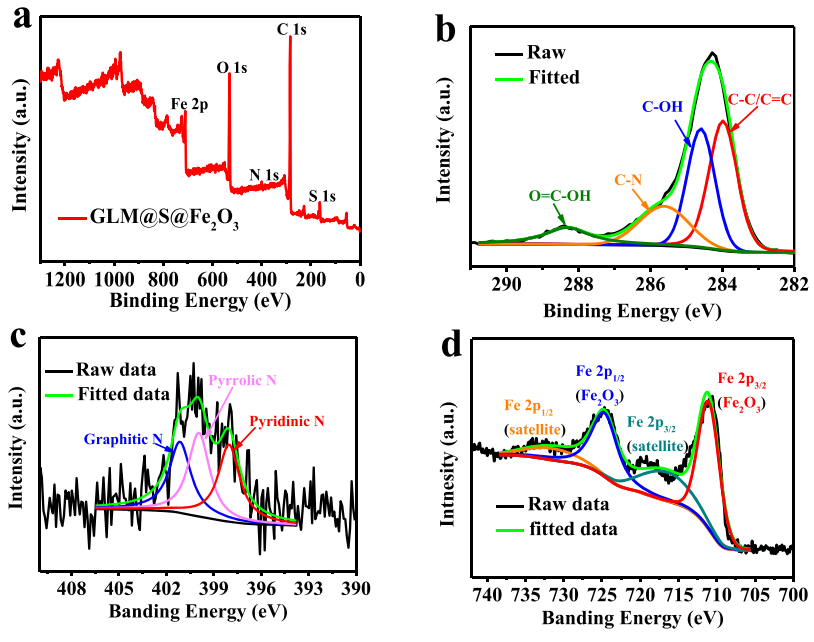

Figure 4. (a) XPS survey scan. High resolution XPS spectra of (b) C 1s, (b) N 1s, and (d) Fe 2p of the GLM@S@Fe_2O_3 composite.

https://dx.doi.org/10.1021/acsanm.9b02250
ACS Appl. Nano Mater. 2020, 3, 1382−1390

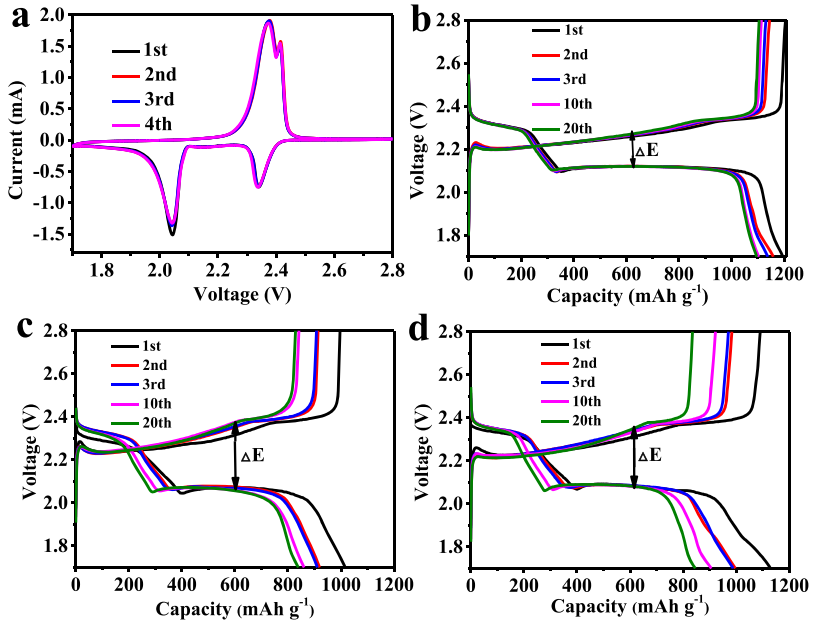

Figure 5. (a) Cyclic voltammetry curves of GLM@S@Fe_2O_3 at a scan rate of 0.1 mV s^{-1} for the first five cycles. Charge−discharge profiles for selected cycles of the Li−S cells with (b) GLM@S@Fe_2O_3, (c) GLM@S@Co_3O_4, and (d) GLM@S electrodes.

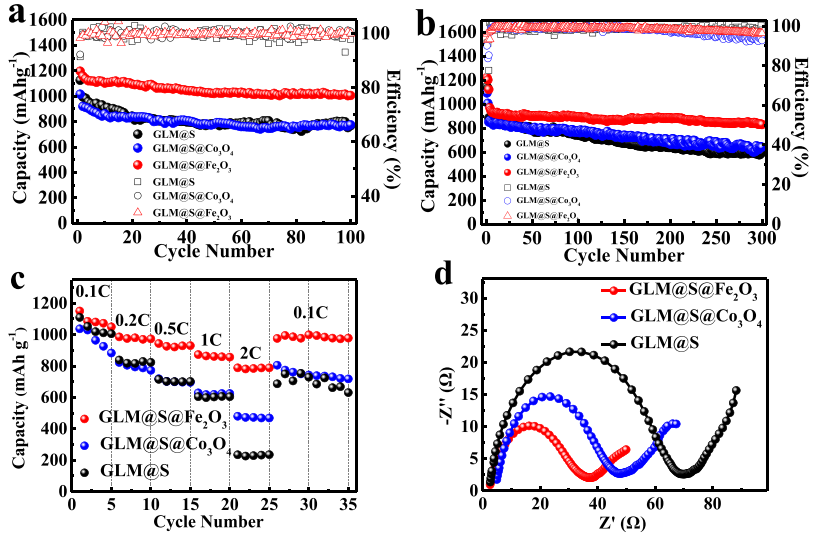

Figure 6. (a) Cycling performances of the GLM@S@Fe_2O_3, GLM@S@Co_3O_4, and GLM@S electrodes at a 0.1C rate for 100 cycles and (b) at a 0.5C rate for 300 cycles. (c) Rate capacity and (d) impedance spectrum of GLM@S@Fe_2O_3, GLM@S@Co_3O_4, and GLM@S.

electrodes (in Figure S4), the ΔE of the GLM@S@Fe_2O_3 electrode is smaller and more stable, suggesting that the redox reaction kinetics and the reversibility of the Li−S battery system are improved.

In order to further confirm the cycling stability of the GLM@S@Fe_2O_3 electrode, the cycle performance was tested at a 0.1C and 0.5C rate between 1.7 and 2.8 V, as displayed in Figure 6a and 6b. At 0.1C, the GLM@S@Fe_2O_3 electrode exhibits more stable cycle performance, and the capacity of GLM@S@Fe_2O_3 can be still stabilized at 1005 mA h g^{-1} after 100 cycles, much higher than that of the GLM@S and GLM@S@Co_3O_4 electrodes. In addition, at 0.5C, the GLM@S@Fe_2O_3 electrode has a discharge capacity of 969 mA h g^{-1} in the fourth cycle (the first three cycles were carried out at the rate of 0.1C for electrode activation), and this capacity slowly fades to 829 mA h g^{-1} after 300 cycles with a slow capacity decay rate of 0.048% per cycle. The GLM@S@Co_3O_4 electrode discharge capacity fades from 863 to 640 mA h g^{-1} with a capacity decay rate of 0.086% per cycle, and similarly, the GLM@S electrode discharge capacity fades from 890 to 596 mA h g^{-1} with a higher capacity decay rate of 0.11% per cycle. Meanwhile, as shown in Figure S5, the electrode of GLM@S@Fe_2O_3 also displays a stable cycling performance at 0.1 and 0.5C under high sulfur loading. Therefore, these results demonstrate that the three-dimensional graphene-like structure GLM@S@Fe_2O_3 can effectively reduce the shuttle effect of lithium polysulfides, as compared with GLM@S and GLM@S@Co_3O_4 hosts. The rate performance was measured with current densities of 0.1, 0.2, 0.5, 1, and 2C. As shown in Figure 6c, the GLM@S@Fe_2O_3 electrode shows greater cycling performance than GLM@S and GLM@S@Co_3O_4, especially at a high current density. At 1 and 2C, the GLM@S@Fe_2O_3

https://dx.doi.org/10.1021/acsanm.9b02250
ACS Appl. Nano Mater. 2020, 3, 1382−1390

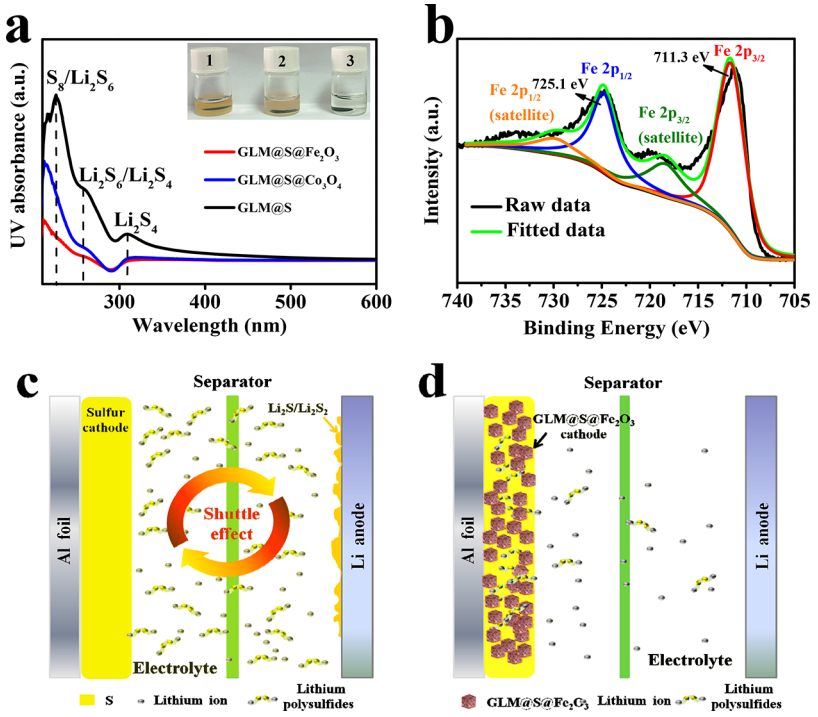

Figure 7. (a) DOL/DME mixed solutions soaked with (1) GLM@S, (2) GLM@S@Co_3O_4, and (3) GLM@S@Fe_2O_3 cathodes after 100 cycles and corresponding UV−vis absorption spectra. (b) The high-resolution XPS spectrum at the Fe 2p region of GLM@S@Fe_2O_3 after 100 cycles. Schematic illustration of Li−S batteries with the (c) sulfur electrode and (d) GLM@S@Fe_2O_3 electrode.

electrode delivers higher discharge capacities of 873 and 788 mA h g^{-1}, respectively, as compared with 628 and 479 mA h g^{-1} for GLM@S@Co_3O_4 and 604 and 234 mA h g^{-1} for GLM@S, respectively. After cycling at incremental rates and switching back to 0.1C, the specific capacity of GLM@S@Fe_2O_3 can still be recovered to 1000 mA h g^{-1}, implying good cycling stability and rate capability. Furthermore, the charge−discharge profiles of Li−S batteries with the GLM@S@Fe_2O_3, GLM@S@Co_3O_4, and GLM@S electrodes at various C rates of 0.1C to 2C are shown in Figure S6. As the current rate increases, the overpotential increases and the discharge plateau decreases. Additionally, compared with GLM@S@Co_3O_4 and GLM@S, the changes of the overpotential and discharge plateau are minimal for GLM@S@Fe_2O_3, especially at current densities of 1 and 2C, indicating that GLM@S@Fe_2O_3 has better electronic conductivity and ionic diffusivity at high rates.[45] These results further illustrate that the GLM@S@Fe_2O_3 electrode has an excellent structural stability and could be used as a high-rate sulfur cathode.

Electrochemical impedance spectroscopy (EIS) was measured within the range of 0.01 to 10^5 Hz. The Nyquist plots show a semicircle in the medium-high frequency range and an inclined slope in the low frequency region, corresponding to the charge-transfer resistance (R_{ct}) at the interface and ion diffusion within the electrode, respectively.[71] As shown in Figure 6d, the GLM@S@Fe_2O_3, GLM@S, and GLM@S@Co_3O_4 composites all have lower R_{ct}, which is attributed to the carbon hosts doped with nitrogen, and the GLM@S@Fe_2O_3 composite has the lowest R_{ct} (36.1 Ω) due to the three-dimensional graphene-like structure used as a conductive network and the adsorption effect of the polysulfides derived from the iron oxide. In order to further investigate the ion diffusion, the Linear Warburg impedance diagram is fitted in Figure S7. A_w (Warburg coefficient) is the linear slope, and the Li^+ diffusion coefficient is proportional to $1/A_w^2$, demonstrating that GLM@S@Fe_2O_3 also has the largest Li^+ diffusion coefficient due to the three-dimensional graphene-like structure for an ion channel.

In order to reveal the mechanism of battery performance enhancement, the electrodes of GLM@S@Fe_2O_3, GLM@S@Co_3O_4, and GLM@S after 100 cycles were immersed in DOL/DME mixed solutions for 8 h. As shown in Figure 7a, the mixed solution containing the GLM@S@Fe_2O_3 electrode appears colorless and transparent. In comparison, the color of the mixed solution containing the GLM@S@Co_3O_4 and GLM@S electrodes are pale yellow and deeper yellow, respectively. These results reveal that the electrode with GLM@S@Fe_2O_3 displays the least amount of polysulfides dissolved in the electrolyte, and the UV−vis absorption spectra shown in Figure 7a further confirm that the GLM@S@Fe_2O_3 host can effectively reduce the polysulfides dissolved in the electrolyte. The weakest absorption peaks of S_8/Li_2S_6, Li_2S_6/Li_2S_4, and Li_2S_4 for GLM@S@Fe_2O_3 demonstrate a minimum for polysulfides dissolved in the electrolyte.[24,67,72] Moreover, the GLM@S@Fe_2O_3 electrode after 100 cycles was investigated by X-ray photoelectron spectroscopy. As shown in Figure 7b, two major peaks at 711.3 and 725.1 eV are derived from Fe $2p_{3/2}$ and Fe $2p_{1/2}$. Compared with the Fe 2p spectrum of fresh GLM@S@Fe_2O_3 in Figure 4d, the GLM@S@Fe_2O_3 composite after 100 cycles shows an overall shift toward a higher binding energy, indicating the strong adsorptivity of Fe_2O_3 toward lithium polysulfides.[73,74] Therefore, the shuttle effect mechanism using the GLM@S@Fe_2O_3 electrode is illustrated in Figure 7c and d. The battery with the GLM@S@Fe_2O_3 electrode shows the ideal state with minimum amounts of lithium sulfides shuttling to the anode, which is mainly attributed to two advantages of the GLM@S@Fe_2O_3 composite. First, the GLM@Fe_2O_3 host with a 3D

https://dx.doi.org/10.1021/acsanm.9b02250
ACS Appl. Nano Mater. 2020, 3, 1382−1390

matrix has a physical buffering effect on the dissolution of lithium polysulfide. Second, the polar nitrogen and Fe_2O_3 strongly adsorb lithium polysulfide, which can further limit the shuttle effect.

4. CONCLUSIONS

In summary, we have successfully synthesized a three-dimensional graphene-like matrix with Fe_2O_3 evenly dispersed on the surface of nanosheets through a simple one-step route. The GLM@S@Fe_2O_3 matrix has a large specific surface area and an ordered space structure, which does much to advantage the sulfur loading, lithium ion transport, and electronic conduction. In addition, the polar nitrogen and Fe_2O_3 have strong adsorption on polysulfides, which restrains the solution and diffusion of the polysulfides. Therefore, when the GLM@S@Fe_2O_3 matrix is applied in the Li−S battery, the as-designed cathode presents an excellent electrochemical performance, delivering an initial specific capacity of 1196 mA h g^{-1} at 0.1C and a high specific discharge capacity of 829 mA h g^{-1} after 300 cycles at 0.5C with a capacity decay as small as 0.048% per cycle. These results demonstrate that the GLM@S@Fe_2O_3 matrix is an ideal host for sulfur in Li−S batteries and is especially suitable for future industrialization applications.

■ ASSOCIATED CONTENT

Supporting Information

The Supporting Information is available free of charge at https://pubs.acs.org/doi/10.1021/acsanm.9b02250.

SEM images, XRD patterns, TG curve, potential difference (ΔE) between the charge and discharge plateaus, cycling performance, charge−discharge profiles of Li−S cells, and linear Warburg impedance diagram (PDF)

■ AUTHOR INFORMATION

Corresponding Authors

Jiasong Zhong − *College of Materials and Environmental Engineering, Hangzhou Dianzi University, Hangzhou 310018, P.R. China*; Email: jiasongzhong@hdu.edu.cn

Tao Yang − *College of Materials and Environmental Engineering, Hangzhou Dianzi University, Hangzhou 310018, P.R. China*; orcid.org/0000-0002-6948-0028; Email: yangtao@hdu.edu.cn

Jianwen Liu − *Hubei Collaborative Innovation Center for Advanced Organic Chemical Materials, Hubei University, Wuhan 430062, P. R. China*; orcid.org/0000-0003-4929-1075; Phone: +86 27 88662747; Email: jianwen@hubu.edu.cn

Authors

Pengyu Wang − *Hubei Collaborative Innovation Center for Advanced Organic Chemical Materials, Hubei University, Wuhan 430062, P. R. China*

Rong Zeng − *Hubei Collaborative Innovation Center for Advanced Organic Chemical Materials, Hubei University, Wuhan 430062, P. R. China*

Lei You − *Hubei Collaborative Innovation Center for Advanced Organic Chemical Materials, Hubei University, Wuhan 430062, P. R. China*

Hu Tang − *Hubei Collaborative Innovation Center for Advanced Organic Chemical Materials, Hubei University, Wuhan 430062, P. R. China*

Shiquan Wang − *Hubei Collaborative Innovation Center for Advanced Organic Chemical Materials, Hubei University, Wuhan 430062, P. R. China*

Complete contact information is available at: https://pubs.acs.org/10.1021/acsanm.9b02250

Author Contributions

#These authors contributed equally to this work.

Notes

The authors declare no competing financial interest.

■ ACKNOWLEDGMENTS

This work was financially supported by the National Natural Science Foundation of China (No. 21706055) and Zhejiang Provincial Natural Science Foundation of China (No. LQ20E020006). The authors would also like to thank the Analytical and Testing Center of Hubei University for providing the facilities to complete the experimental measurements. Technical support from Hubei Nuobang Chemical Company Co. Ltd. is also gratefully acknowledged.

■ REFERENCES

(1) Alias, N.; Mohamad, A. A. Advances of aqueous rechargeable lithium-ion battery: A review. *J. Power Sources* **2015**, *274*, 237−251.

(2) Kang, W.; Deng, N.; Ju, J.; Li, Q.; Wu, D.; Ma, X.; Li, L.; Naebe, M.; Cheng, B. A review of recent developments in rechargeable lithium-sulfur batteries. *Nanoscale* **2016**, *8*, 16541−16588.

(3) Eroglu, D.; Zavadil, K. R.; Gallagher, K. G. Critical link between materials chemistry and cell-level design for high energy density and low cost lithium-sulfur transportation battery. *J. Electrochem. Soc.* **2015**, *162*, A982−A990.

(4) Li, C.; Liu, X.; Zhu, L.; Huang, R.; Zhao, M.; Xu, L.; Qian, Y. Conductive and polar titanium boride as a sulfur host for advanced lithium-sulfur batteries. *Chem. Mater.* **2018**, *30*, 6969−6977.

(5) Liu, X.; Huang, J. Q.; Zhang, Q.; Mai, L. Nanostructured metal oxides and sulfides for lithium-sulfur batteries. *Adv. Mater.* **2017**, *29*, 1601759.

(6) Jayaprakash, N.; Shen, J.; Moganty, S. S.; Corona, A.; Archer, L. A. Porous hollow carbon@sulfur composites for high-power lithium-sulfur batteries. *Angew. Chem., Int. Ed.* **2011**, *50*, 5904−5908.

(7) Li, X.; Cheng, X.; Gao, M.; Ren, D.; Liu, Y.; Guo, Z.; Shang, C.; Sun, L.; Pan, H. Amylose-derived macrohollow core and microporous shell carbon spheres as sulfur host for superior lithium-sulfur battery cathodes. *ACS Appl. Mater. Interfaces* **2017**, *9*, 10717−10729.

(8) Liu, Y.; Li, G.; Fu, J.; Chen, Z.; Peng, X. Strings of porous carbon polyhedrons as self-standing cathode host for high-energy-density lithium-sulfur batteries. *Angew. Chem., Int. Ed.* **2017**, *56*, 6176−6180.

(9) Li, G.; Lei, W.; Luo, D.; Deng, Y. P.; Wang, D.; Chen, Z. Highly conductive, light weight, robust, corrosion-resistant, scalable, all-fiber based current collectors for aqueous acidic batteries. *Adv. Energy Mater.* **2018**, *8*, 1702381.

(10) Hu, C.; Kirk, C.; Cai, Q.; Cuadrado-Collados, C.; Silvestre-Albero, J.; Rodriguez-Reinoso, F.; Biggs, M. J. A high-volumetric-capacity cathode based on interconnected close-packed N-doped porous carbon nanospheres for long-life lithium-sulfur batteries. *Adv. Energy Mater.* **2017**, *7*, 1701082.

(11) Chyan, Y.; Ye, R.; Li, Y.; Singh, S. P.; Arnusch, C. J.; Tour, J. M. Laser-induced graphene by multiple lasing: toward electronics on cloth, paper, and food. *ACS Nano* **2018**, *12*, 2176−2183.

(12) Mi, K.; Chen, S.; Xi, B.; Kai, S.; Jiang, Y.; Feng, J.; Qian, Y.; Xiong, S. Sole chemical confinement of polysulfides on nonporous nitrogen/oxygen dual-doped carbon at the kilogram scale for lithium-sulfur batteries. *Adv. Funct. Mater.* **2017**, *27*, 1604265.

(13) Liang, X.; Zhang, M.; Kaiser, M. R.; Gao, X.; Konstantinov, K.; Tandiono, R.; Wang, Z.; Liu, H.-K.; Dou, S.-X.; Wang, J. Split-half-tubular polypyrrole@sulfur@polypyrrole composite with a novel

three-layer-3D structure as cathode for lithium/sulfur batteries. *Nano Energy* **2015**, *11*, 587−599.
(14) Peng, H. J.; Wang, D. W.; Huang, J. Q.; Cheng, X. B.; Yuan, Z.; Wei, F.; Zhang, Q. Janus separator of polypropylene-supported cellular graphene framework for sulfur cathodes with high utilization in lithium-sulfur batteries. *Adv. Sci.* **2016**, *3*, 1500268.
(15) Li, X.; Ding, K.; Gao, B.; Li, Q.; Li, Y.; Fu, J.; Zhang, X.; Chu, P. K.; Huo, K. Freestanding carbon encapsulated mesoporous vanadium nitride nanowires enable highly stable sulfur cathodes for lithium-sulfur batteries. *Nano Energy* **2017**, *40*, 655−662.
(16) Wu, W.; Pu, J.; Wang, J.; Shen, Z.; Tang, H.; Deng, Z.; Tao, X.; Pan, F.; Zhang, H. Biomimetic bipolar microcapsules derived from staphylococcus aureus for enhanced properties of lithium-sulfur battery cathodes. *Adv. Energy Mater.* **2018**, *8*, 1702373.
(17) Yilmaz, G.; Lu, X.; Ho, G. W. Cross-linker mediated formation of sulfur-functionalized V_2O_5/graphene aerogels and their enhanced pseudocapacitive performance. *Nanoscale* **2017**, *9*, 802−811.
(18) Lee, J.; Hwang, T.; Lee, Y.; Lee, J. K.; Choi, W. Coating of sulfur particles with manganese oxide nanowires as a cathode material in lithium-sulfur batteries. *Mater. Lett.* **2015**, *158*, 132−135.
(19) Wang, J.; Liang, J.; Wu, J.; Xuan, C.; Wu, Z.; Guo, X.; Lai, C.; Zhu, Y.; Wang, D. Coordination effect of network NiO nanosheet and a carbon layer on the cathode side in constructing a high-performance lithium−sulfur battery. *J. Mater. Chem. A* **2018**, *6*, 6503−6509.
(20) Mosavati, N.; Salley, S. O.; Ng, K. Y. S. Characterization and electrochemical activities of nanostructured transition metal nitrides as cathode materials for lithium sulfur batteries. *J. Power Sources* **2017**, *340*, 210−216.
(21) Hao, Z.; Yuan, L.; Chen, C.; Xiang, J.; Li, Y.; Huang, Z.; Hu, P.; Huang, Y. TiN as a simple and efficient polysulfide immobilizer for lithium-sulfur batteries. *J. Mater. Chem. A* **2016**, *4*, 17711−17717.
(22) Liu, Z.; Zheng, X.; Luo, S.-l.; Xu, S.-q.; Yuan, N.-y.; Ding, J.-n. High performance Li-S battery based on amorphous NiS_2 as the host material for the S cathode. *J. Mater. Chem. A* **2016**, *4*, 13395−13399.
(23) Xiao, Z.; Yang, Z.; Zhang, L.; Pan, H.; Wang, R. Sandwich-type NbS_2@S@I-doped graphene for high-sulfur-loaded, ultrahigh-rate, and long-life lithium-sulfur batteries. *ACS Nano* **2017**, *11*, 8488−8498.
(24) Chen, T.; Zhang, Z.; Cheng, B.; Chen, R.; Hu, Y.; Ma, L.; Zhu, G.; Liu, J.; Jin, Z. Self-templated formation of interlaced carbon nanotubes threaded hollow Co_3S_4 nanoboxes for high-rate and heat-resistant lithium-sulfur batteries. *J. Am. Chem. Soc.* **2017**, *139*, 12710−12715.
(25) Hao, G.-P.; Tang, C.; Zhang, E.; Zhai, P.; Yin, J.; Zhu, W.; Zhang, Q.; Kaskel, S. Thermal exfoliation of layered metal-organic frameworks into ultrahydrophilic graphene stacks and their applications in Li-S batteries. *Adv. Mater.* **2017**, *29*, 1702829.
(26) Yang, M.; Hu, X.; Fang, Z.; Sun, L.; Yuan, Z.; Wang, S.; Hong, W.; Chen, X.; Yu, D. Bifunctional MOF-derived carbon photonic crystal architectures for advanced Zn-Air and Li-S batteries: highly exposed graphitic nitrogen matters. *Adv. Funct. Mater.* **2017**, *27*, 1701971.
(27) Cao, J.; Chen, C.; Zhao, Q.; Zhang, N.; Lu, Q.; Wang, X.; Niu, Z.; Chen, J. A flexible nanostructured paper of a reduced graphene oxide-sulfur composite for high-performance lithium-sulfur batteries with unconventional configurations. *Adv. Mater.* **2016**, *28*, 9629−9636.
(28) Zhang, Z.; Li, Z.; Hao, F.; Wang, X.; Li, Q.; Qi, Y.; Fan, R.; Yin, L. 3D interconnected porous carbon aerogels as sulfur immobilizers for sulfur impregnation for lithium-sulfur batteries with high rate capability and cycling stability. *Adv. Funct. Mater.* **2014**, *24*, 2500−2509.
(29) Yuan, Z.; Peng, H. J.; Huang, J. Q.; Liu, X. Y.; Wang, D. W.; Cheng, X. B.; Zhang, Q. Hierarchical free-standing carbon-nanotube paper electrodes with sltrahigh sulfur-loading for lithium-sulfur batteries. *Adv. Funct. Mater.* **2014**, *24*, 6105−6112.
(30) Peng, H. J.; Hou, T. Z.; Zhang, Q.; Huang, J. Q.; Cheng, X. B.; Guo, M. Q.; Yuan, Z.; He, L. Y.; Wei, F. Strongly coupled interfaces between a heterogeneous carbon host and a sulfur-containing guest for highly stable lithium-sulfur batteries: mechanistic insight into capacity degradation. *Adv. Mater. Interfaces* **2014**, *1*, 1400227.
(31) Hwang, J. Y.; Kim, H. M.; Shin, S.; Sun, Y. K. Designing a high-performance lithium-sulfur batteries based on layered double hydroxides-carbon nanotubes composite cathode and a dual-functional graphene-polypropylene-Al_2O_3 separator. *Adv. Funct. Mater.* **2018**, *28*, 1704294.
(32) Qi, S.; Sun, J.; Ma, J.; Sun, Y.; Goossens, K.; Li, H.; Jia, P.; Fan, X.; Bielawski, C. W.; Geng, J. Covalent bonding of sulfur nanoparticles to unzipped multiwalled carbon nanotubes for high-performance lithium-sulfur batteries. *Nanotechnology* **2019**, *30*, No. 024001.
(33) Peng, H. J.; Huang, J. Q.; Zhao, M. Q.; Zhang, Q.; Cheng, X. B.; Liu, X. Y.; Qian, W. Z.; Wei, F. Nanoarchitectured graphene/CNT@porous carbon with extraordinary electrical conductivity and interconnected micro/mesopores for lithium-sulfur batteries. *Adv. Funct. Mater.* **2014**, *24*, 2772−2781.
(34) Xiao, P.; Bu, F.; Yang, G.; Zhang, Y.; Xu, Y. Integration of graphene, nano sulfur, and conducting polymer into compact, flexible lithium-sulfur battery cathodes with ultrahigh volumetric capacity and superior cycling stability for foldable devices. *Adv. Mater.* **2017**, *29*, 1703324.
(35) Li, G.; Sun, J.; Hou, W.; Jiang, S.; Huang, Y.; Geng, J. Three-dimensional porous carbon composites containing high sulfur nanoparticle content for high-performance lithium-sulfur batteries. *Nat. Commun.* **2016**, *7*, 10601.
(36) Sun, Y.; Ma, J.; Yang, X.; Wen, L.; Zhou, W.; Geng, J. Sulfur covalently bonded to porous graphitic carbon as an anode material for lithium-ion capacitors with high energy storage performance. *J. Mater. Chem. A* **2020**, *8*, 62−68.
(37) Ma, J.; Fan, J.; Chen, S.; Yang, X.; Hui, K. N.; Zhang, H.; Bielawski, C. W.; Geng, J. Covalent confinement of sulfur copolymers onto graphene sheets affords ultrastable lithium-sulfur batteries with fast cathode kinetics. *ACS Appl. Mater. Interfaces* **2019**, *11*, 13234−13243.
(38) Zhong, Y.; Xia, X.; Deng, S.; Zhan, J.; Fang, R.; Xia, Y.; Wang, X.; Zhang, Q.; Tu, J. Popcorn inspired porous macrocellular carbon: rapid puffing fabrication from rice and its applications in lithium-sulfur batteries. *Adv. Energy Mater.* **2018**, *8*, 1701110.
(39) Dutta, S.; Bhaumik, A.; Wu, K. C. Hierarchically porous carbon derived from polymers and biomass: effect of interconnected pores on energy applications. *Energy Environ. Sci.* **2014**, *7*, 3574−3592.
(40) Shen, K.; Mei, H.; Li, B.; Ding, J.; Yang, S. 3D printing sulfur copolymer-graphene architectures for Li-S batteries. *Adv. Energy Mater.* **2018**, *8*, 1701527.
(41) Hwa, Y.; Seo, H. K.; Yuk, J. M.; Cairns, E. J. Freeze-dried sulfur-graphene oxide-carbon nanotube nanocomposite for high sulfur-loading lithium/sulfur cells. *Nano Lett.* **2017**, *17*, 7086−7094.
(42) Zhao, C.; Shen, C.; Xin, F.; Sun, Z.; Han, W. Prussian blue-derived Fe_2O_3/sulfur composite cathode for lithium-sulfur batteries. *Mater. Lett.* **2014**, *137*, 52−55.
(43) Ni, L. B.; Zhao, G. J.; Yang, G.; Niu, G. S.; Chen, M.; Diao, G. W. Dual core-shell-structured S@C@MnO_2 nanocomposite for highly stable lithium−sulfur batteries. *ACS Appl. Mater. Interfaces* **2017**, *9*, 34793−34803.
(44) Chen, H.; Dong, W.-D.; Xia, F.-J.; Zhang, Y.-J.; Yan, M.; Song, J.-P.; Zou, W.; Liu, Y.; Hu, Z.-Y.; Liu, J.; Li, Y.; Wang, H.-E.; Chen, L.-H.; Su, B.-L. Hollow nitrogen-doped carbon/sulfur@MnO_2 nanocomposite with structural and chemical dual-encapsulation for lithium-sulfur battery. *Chem. Eng. J.* **2020**, *381*, 122746.
(45) Song, X.; Gao, T.; Wang, S. Q.; Bao, Y.; Chen, G. P.; Ding, L. X.; Wang, H. H. Free-standing sulfur host based on titanium-dioxide-modified porous-carbon nanofibers for lithium-sulfur batteries. *J. Power Sources* **2017**, *356*, 172−180.
(46) Jiao, L.; Zhang, C.; Geng, C.; Wu, S.; Li, H.; Lv, W.; Tao, Y.; Chen, Z.; Zhou, G.; Li, J.; Ling, G.; Wan, Y.; Yang, Q.-H. Capture and Catalytic Conversion of Polysulfides by In Situ Built TiO_2-MXene Heterostructures for Lithium-Sulfur Batteries. *Adv. Energy Mater.* **2019**, *9*, 1900219.

https://dx.doi.org/10.1021/acsanm.9b02250
ACS Appl. Nano Mater. 2020, 3, 1382−1390

(47) Gao, X. T.; Xie, Y.; Zhu, X. D.; Sun, K. N.; Xie, X. M.; Liu, Y. T.; Yu, J. Y.; Ding, B. Ultrathin MXene Nanosheets Decorated with TiO2 Quantum Dots as an Efficient Sulfur Host toward Fast and Stable Li-S Batteries. *Small* **2018**, *14*, 1802443.
(48) Li, N.; Chen, Z. X.; Chen, F.; Hu, G. J.; Wang, S. G.; Sun, Z. H.; Sun, X. D.; Li, F. From interlayer to lightweight capping layer: Rational design of mesoporous TiO_2 threaded with CNTs for advanced Li-S batteries. *Carbon* **2019**, *143*, 523−530.
(49) Razaq, R.; Sun, D.; Xin, Y.; Li, Q.; Huang, T. Z.; Zhang, Z. L.; Huang, Y. H. Nanoparticle assembled mesoporous MoO_2 microrods derived from metal organic framework and wrapped with graphene as the sulfur host for long-life lithium-sulfur batteries. *Adv. Mater. Interfaces* **2019**, *6*, 1801636.
(50) Xiang, M. W.; Wu, H.; Liu, H.; Huang, J.; Zheng, Y. F.; Yang, L.; Jing, P.; Zhang, Y.; Dou, S. X.; Liu, H. K. A Flexible 3D multifunctional MgO-decorated carbon foam@CNTs hybrid as self-supported cathode for high-performance lithium-sulfur batteries. *Adv. Funct. Mater.* **2017**, *27*, 1702573.
(51) Wang, H. Q.; Zhou, T. F.; Li, D.; Gao, H.; Gao, G. P.; Du, A. J.; Liu, H. K.; Guo, Z. P. Ultrathin cobaltosic oxide nanosheets as an effective sulfur encapsulation matrix with strong affinity toward polysulfides. *ACS Appl. Mater. Interfaces* **2017**, *9*, 4320−4325.
(52) He, J.; Luo, L.; Chen, Y.; Manthiram, A. Yolk-shelled C@Fe_3O_4 nanoboxes as efficient sulfur hosts for high-performance lithium-sulfur batteries. *Adv. Mater.* **2017**, *29*, 1702707.
(53) Gao, H.; Zhou, T.; Zheng, Y.; Liu, Y.; Chen, J.; Liu, H.; Guo, Z. P. Integrated carbon/red phosphorus/graphene aerogel 3D architecture via advanced vapor-redistribution for high-energy sodium-ion batteries. *Adv. Energy Mater.* **2016**, *6*, 1601037. (2016)
(54) Liang, X.; Kwok, C. Y.; Lodi-Marzano, F.; Pang, Q.; Cuisinier, M.; Huang, H.; Hart, C. J.; Houtarde, D.; Kaup, K.; Sommer, H.; Brezesinski, T.; Janek, J.; Nazar, L. F. Tuning transition metal oxide-sulfur interactions for long life lithium sulfur batteries: The "Goldilocks" principle. *Adv. Energy Mater.* **2016**, *6*, 1501636.
(55) Martin, R. B. Citrate binding of Al^{3+} and Fe^{3+}. *J. Inorg. Biochem.* **1986**, *28*, 181−187.
(56) Silva, A. M. N.; Kong, X.; Parkin, M. C.; Cammack, R.; Hider, R. C. Iron (III) citrate speciation in aqueous solution. *Dalton Trans.* **2009**, *70*, 8616−8625.
(57) Kotsakis, N.; Raptopoulou, C. P.; Tangoulis, V.; Terzis, A.; Giapintzakis, J.; Jakusch, T.; Kiss, T.; Salifoglou, A. Correlations of synthetic, spectroscopic, structural, and speciation studies in the biologically relevant cobalt (II)-citrate System: the tale of the first aqueous dinuclear cobalt (II)-citrate complex. *Inorg. Chem.* **2003**, *42*, 22−31.
(58) Chen, J.; Xiao, Y.; Huang, B.; Sun, X. Sustainable cool pigments based on iron and tungsten co-doped lanthanum cerium oxide with high NIR reflectance for energy saving. *Dyes Pigm.* **2018**, *154*, 1−7.
(59) Yang, T.; Liu, Y.; Yang, D.; Deng, B.; Huang, Z.; Ling, C. D.; Liu, H.; Wang, G. X.; Guo, Z. P.; Zheng, R. K. Bimetallic metal-organic frameworks derived Ni-Co-Se@C hierarchical bundle-like nanostructures with high-rate pseudocapacitive lithium ion storage. *Energy Storage Mater.* **2019**, *17*, 374−384.
(60) Yuan, H. D.; Zhang, W. K.; Wang, J. G.; Zhou, G. M.; Zhuang, Z. Z.; Luo, J. M.; Huang, H.; Gan, Y. P.; Liang, C.; Xia, Y.; Zhang, J.; Tao, X. Y. Facilitation of sulfur evolution reaction by pyridinic nitrogen doped carbon nanoflakes for highly-stable lithium-sulfur batteries. *Energy Storage Mater.* **2018**, *10*, 1−9.
(61) Lu, K.; Zhang, H.; Gao, S.; Ma, H.; Chen, J.; Cheng, Y. Manipulating polysulfide conversion with strongly coupled Fe_3O_4 and nitrogen doped carbon for stable and high capacity lithium-sulfur batteries. *Adv. Funct. Mater.* **2019**, *29*, 1807309.
(62) Lai, L.; Chen, L.; Zhan, D.; Sun, L.; Liu, J.; Lim, S. H.; Poh, C. K.; Shen, Z.; Lin, J. One-step synthesis of NH_2-graphene from in situ graphene-oxide reduction and its improved electrochemical properties. *Carbon* **2011**, *49*, 3250−3257.
(63) Park, S. K.; Lee, J. K.; Kang, Y. C. Yolk-shell structured assembly of bamboo-like nitrogen-doped carbon nanotubes embedded with Co nanocrystals and their application as cathode material for Li-S batteries. *Adv. Funct. Mater.* **2018**, *28*, 1705264. (2016)
(64) Zhou, G.; Zhao, Y.; Manthiram, A. Dual-confined flexible sulfur cathodes encapsulated in nitrogen-doped double-shelled hollow carbon spheres and wrapped with graphene for Li-S batteries. *Adv. Energy Mater.* **2015**, *5*, 1402263.
(65) Yang, K.; Zhong, L.; Qin, J. X.; Liu, J. C.; Xiao, M.; Han, D. M.; Ren, S.; Sun, L. Y.; Wang, S. J.; Meng, Y. Z. In Situ Laminated Separator Using Nitrogen−Sulfur Codoped Two-Dimensional Carbon Material to Anchor Polysulfides for High-Performance Li−S Batteries. *ACS Appl. Nano Mater.* **2018**, *1*, 3807−3816.
(66) Sun, J.; Ma, J.; Fan, J.; Pyun, J.; Geng, J. Rational design of sulfur-containing composites for high-performance lithium-sulfur batteries. *APL Mater.* **2019**, *7*, No. 020904.
(67) Wang, H.; Zhang, W.; Liu, H.; Guo, Z. A strategy for configuration of an integrated flexible sulfur cathode for high-performance lithium-sulfur batteries. *Angew. Chem., Int. Ed.* **2016**, *55*, 3992−3996.
(68) Cuisinier, M.; Cabelguen, P.-E.; Evers, S.; He, G.; Kolbeck, M.; Garsuch, A.; Bolin, T.; Balasubramanian, M.; Nazar, L. F. Sulfur speciation in Li-S batteries determined by operando X-ray absorption spectroscopy. *Chem. Lett.* **2013**, *4*, 3227−3232.
(69) Lu, Y.-C.; He, Q.; Gasteiger, H. A. Probing the lithium-sulfur redox reactions: a rotating-ring disk electrode study. *J. Phys. Chem. C* **2014**, *118*, 5733−5741.
(70) Wild, M.; O'Neill, L.; Zhang, T.; Purkayastha, R.; Minton, G.; Marinescu, M.; Offer, G. J. Lithium sulfur batteries, a mechanistic review. *Energy Environ. Sci.* **2015**, *8*, 3477−3494.
(71) Yuan, Z.; Peng, H. J.; Hou, T. Z.; Huang, J. Q.; Chen, C. M.; Wang, D. W.; Cheng, X. B.; Wei, F.; Zhang, Q. Powering lithium-sulfur battery performance by propelling polysulfide redox at sulfiphilic hosts. *Nano Lett.* **2016**, *16*, 519−527.
(72) Lu, K.; Liu, Y.; Chen, J.; Zhang, Z.; Cheng, Y. Redox catalytic and quasi-solid sulfur conversion for high-capacity lean lithium sulfur batteries. *ACS Nano* **2019**, *13*, 14540−14548.
(73) Chen, T.; Zhang, Z.; Cheng, B.; Chen, R.; Hu, Y.; Ma, L.; Zhu, G.; Liu, J.; Jin, Z. Self-templated formation of interlaced carbon nanotubes threaded hollow Co_3S_4 nanoboxes for high-rate and heat-resistant lithium-sulfur batteries. *J. Am. Chem. Soc.* **2017**, *139*, 12710−12715.
(74) Wang, Z.; Shen, J.; Liu, J.; X, Xu.; Liu, Z.; R, Hu.; Ouyang, L. Self-supported and flexible sulfur cathode enabled via synergistic confinement for high-energy-density lithium-sulfur batteries. *Adv. Mater.* **2019**, 1902228.

https://dx.doi.org/10.1021/acsanm.9b02250
ACS Appl. Nano Mater. 2020, 3, 1382−1390